1 **Revisiting the Detection of Optical Lightning Superbolts**

2 **Michael Peterson[1], Matt W. Kirkland[2]**
3
4
5 [1]ISR-2, Los Alamos National Laboratory, Los Alamos, New Mexico
6 [2]A-Division, Los Alamos National Laboratory, Los Alamos, New Mexico

7

8

9

10

11

12 Corresponding author: Michael Peterson (mpeterson@lanl.gov), B241, P.O. Box 1663 Los
13 Alamos, NM, 87545

14

15

16 **Key Points:**

17 • Optical superbolts are identified based on peak optical power. Short-duration superbolts
18 may be missed if defined by total energy

19 • Normal lightning produces optical superbolts worldwide, but these superbolts are
20 relatively weak - near the 100 GW threshold

21 • Powerful (>350 GW) optical superbolts result preferentially from +CGs and are often
22 found in oceanic wintertime storms

23
24

25   **Abstract**

26   This study uses Fast On-Orbit Detection of Transient Events (FORTE) satellite
27   observations to identify superbolt-class optical lightning events and evaluate their origins.
28   Superbolts have been defined by Turman (1977) as lightning pulses whose peak optical power
29   exceeds 10^{11} W. However, it has been unclear whether superbolts resulted from particular types
30   of high-energy lightning process or whether they were the result of measurement bias. In the
31   latter case, any decently-bright lightning process could be recorded as a superbolt if the sensor
32   had a particularly clear sight line to the hot channel without thick clouds diluting the optical
33   signals.
34   Our 12-year analysis of FORTE superbolt detections indicates that the lower optical
35   superbolt energy range (~100 GW) is dominated by normal lightning, but brighter cases are
36   predominantly strong +CG strokes that originate from specific types of storms. Oceanic storm
37   systems, particularly during the winter, and especially those located around Japan are shown to
38   produce these intense superbolts. We suggest that some optical superbolts result from favorable
39   viewing conditions and would not be identified as such by another instrument located elsewhere,
40   and that others are associated with a unique set of physics that may merit the "superbolt"
41   distinction.
42
43

44   **Plain Language Summary**

45   In 1977, Turman identified lightning that was 100 times brighter than normal in the Vela

46   satellite data. These pulses radiated between 100 GW and multiple terawatts of optical power at

47   the source. This observation sparked a debate as to whether these "superbolts" were caused by a

48   certain type of powerful lightning, or were merely the result of measurement biases. Clouds

49   dilute the optical signals generated by lightning, and reduce the optical powers recorded by

50   satellites. If lightning occurs at the edge of the storm, then the light can travel to the space-based

51   sensor at full intensity. Thus, any lightning event could produce a superbolt if the satellite

52   happened to be in a favorable position to see it, and sensors elsewhere might not classify it as a

53   superbolt.

54   This study analyzes FORTE satellite data to garner a better understanding of optical

55   superbolts. We find that weaker superbolts (100 GW) result from both scenarios: some come

56   from normal lightning, while others are caused by strong +CG strokes that tend to occur in

57   oceanic regions, in the winter, and often near the coast of Japan. The most powerful superbolts

58   (>350 GW), however, predominantly come from strong +CGs and may still merit the "superbolt"

59   distinction.

60

61 **1 Introduction**

62   The most energetic lightning emissions have been termed "superbolts," outshining

63 normal lightning by a factor of 100 or greater. The first measurement of a superbolt was made by

64 the optical payload on the Vela satellite constellation, which was designed to detect nuclear

65 explosions from space. Turman (1977) defined superbolts as having an estimated source optical

66 power of at least 10^{11} W.

67   This designation of a certain class of optical lightning emissions as superbolts initiated a

68 debate in the lightning research community as to whether these highly-radiance events resulted

69 from some undiscovered exotic lightning process (new physics), whether they were produced by

70 a particular type of lightning event enabled by favorable conditions in the electrified cloud

71 (unique physics), or whether superbolts were just normal lightning in ordinary storms that

72 happen to have been observed by an on-orbit sensor with an unobstructed view of the hot

73 lightning channel (normal lightning). If these events represented a new or unique set of physics,

74 then the "superbolt" designation may be appropriate. If superbolts are simply the result of

75 measurement bias from particularly favorable viewing conditions (rather than lightning physics),

76 then it is not warranted. Over the past four decades, evidence has accumulated that supports both

77 concepts.

78 1.1 Superbolts as a unique type of lightning

79   The case for superbolts representing a unique set of physics is built on similarities

80 between Turman's superbolt Vela waveforms and ground-based optical measurements of

81 positive-polarity cloud-to-ground (CG) strokes taken by Berger and Vogelsanger (1969), as well

82 as a geographic and seasonal preference for superbolt activity over Japan and the northern

83   Pacific Ocean during the winter months. This wintertime oceanic preference for superbolts

84   differs from the behavior of normal lightning that primarily occurs over land during the warm

85   season (Cecil et al., 2014) and usually produces negative-polarity CG strokes (Rakov, 2003).

86   While land-based storms produce frequent lightning and neutralize charge imbalances

87   with each flash, oceanic storms have low flash rates and thus continue to build charge separation

88   over long periods of time. Above-cloud aircraft electric field measurements have shown that

89   oceanic thunderstorms generate steady-state conduction currents (Wilson currents) that are 1.7x

90   stronger than their land-based counterparts (Mach et al., 2010) despite producing less lightning.

91   This discrepancy in the Direct Current (DC) supplied by land and ocean storms to the Global

92   Electric Circuit (GEC) helps to explain why the diurnal cycle of lightning disagrees with the

93   daily change in the fair-weather electric field (the Carnegie curve) (Mach et al., 2011).

94   Thunderstorm dynamics and the resulting precipitation structure of electrified weather differs

95   between land and ocean. Accounting for these structural differences using space-based radar and

96   passive microwave observations leads to the closest reconstruction of the Carnegie curve from

97   supply-side GEC measurements to date (Peterson et al., 2017a). This approach additionally

98   confirms the aircraft-based finding that Wilson currents from oceanic thunderstorms are 1.7x

99   greater than land-based storms (Peterson et al., 2018).

100   With oceanic storms accumulating large amounts of charge before initiating lightning, it

101   is not surprising that oceanic flashes can be particularly powerful when they do occur. Peterson

102   and Liu (2013) used optical Lightning Imaging Sensor (LIS: Christian et al., 2000)

103   measurements to show that oceanic regions produced particularly bright optical lightning flashes

104   that illuminated large areas of the surrounding storm, and that the strength and cloud-top extent

105   of the optical emissions correlated with the lightning peak current reported by matched National

106   Lightning Detection Network (NLDN: Cummins et al., 1998) CG strokes. Peterson et al. (2017b)

107   later refined these results to demonstrate that oceanic flashes were still larger and more radiant

108   than their land-based counterparts when they illuminated similar clouds under the same

109   background illumination. The oceanic preference for optically bright lightning thus arises from

110   physical differences in the flashes produced by oceanic storms, not from viewing conditions

111   affecting the measurements.

112   The wintertime lightning off the coast of Japan that is tied to superbolt activity is a

113   special case of oceanic lightning due to the influence of nearby Siberia on thunderstorm

114   organization and structure. The Sea of Japan and the Pacific Ocean are prone to cold air outbreak

115   events that generate notably shallow storms with cloud-top heights near 4 km, radar echoes

116   extending up to 3 km, and freezing levels near or below the surface. Frontal systems further east

117   over the Pacific may reach 8 km in height with a melting layer extending below 4 km

118   (Yamamoto et al., 2006). Turman (1978) attributed the superbolts detected by Vela in the region

119   to this specific type of weather pattern. In one case, the superbolt originated near the frontal

120   occlusion in a thunderstorm with cloud-top heights of 5.5 km.

121   These vertically-compressed wintertime thunderstorms are known to produce large

122   fractions of anomalous positive-polarity lightning flashes (Miyake et al., 1992). Positive-polarity

123   CG lightning is fundamentally different from its -CG counterpart. For net positive charge to be

124   transferred to the ground, the lightning channel must access a positive charge reservoir within the

125   cloud. This often occurs in bolts from the blue (Rust et al., 1981), while the storm is dissipating

126   (Mazur et al., 1998), or when lightning accesses an electrified stratiform region in a Mesoscale

127   Convective System (MCS) (Lang et al., 2004, 2017). In stratiform cases, the lightning channels

128   can extend horizontally over hundreds of kilometers with their dendritic structures encompassing

129   a charge region that is up to a hundred thousand square kilometers in area (Peterson, 2019a). The

130   largest of these stratiform flashes that has been observed was 709 km in horizontal extent, while

131   the longest-lasting flash was 16.73 s in duration (Peterson et al., 2020a). Enormous amounts of

132   charge from across vast regions can then be funneled down the vertical channels once they attach

133   to ground. +CGs are usually comprised of a single stroke with continuing current that produces

134   broad optical and Radio Frequency (RF) pulses that are hundreds of microseconds in duration

135   (Rakov, 2003). +CGs are thought to generate strong secondary electric fields above the cloud

136   that also lead to the generation of sprites (Pasko et al., 1995,1997). Sprites have been observed in

137   the wintertime oceanic storms near Japan associated with superbolts, even when these storms are

138   smaller than the minimum size threshold required for sprite activity in the continental United

139   States (Hayakawa et al., 2004). Blanc et al. (2007) additionally linked superbolt activity with the

140   production of such transient luminous events (TLEs). If superbolts primarily arise from these

141   intense +CG strokes, then their distinction may well be justified.

142   1.2 Superbolts as normal lightning

143   The case for ordinary lightning generating superbolts is based on the cloud layer between

144   the emissions source and the observing satellite diluting the optical signals via scattering and

145   absorption (Light et al., 2001a). If the lightning flash occurs under a thick layer of cloud, very

146   little light will transmit through the cloud top to reach the satellite (Peterson, 2019b). This causes

147   some lightning activity to be missed by optical space-based lightning imagers (Thomas et al.,

148   2000). However, if a high-current lightning process like a stroke or K-change occurs near the

149   edge of a cloud, the optical emissions can transmit to the satellite at full intensity. In this way,

150   any optically bright CG or IC process could generate a superbolt if the viewing conditions

151   happen to be particularly favorable.

152   One situation where this might arise is when the space-based lightning imager is located

153   near the horizon. If the elevation angle of the satellite is low enough, then the instrument may be

154   able to see below the anvil shield and directly record the undiluted emissions from the exposed

155   lightning channels in CG strokes. For satellites at higher elevation angles, optical emissions from

156   sources near the sides of the storm can still reflect off of neighboring clouds to reach the satellite

157   without transmitting through the full cloud depth. In either case, the signals recorded by the

158   space-based lightning imager will be particularly bright and may reach the superbolt threshold. If

159   superbolts are merely the result of viewing conditions and the geometry of the measurements

160   rather than the underlying physics of the discharge, then the superbolt designation would not be

161   merited. A second sensor at a different location would likely not classify the same optical pulse

162   as a superbolt.

163   Turman (1977) noted this possibility and observed that only 20% of his superbolts were

164   detected by multiple Vela satellites, which were positioned at different azimuth and elevation

165   angles around the source. This fraction of reporting satellites was consistent with Lund's (1973)

166   previous estimates for the probability that a flash would have a clear line-of-sight to a given

167   satellite. Kirkland's (1999) study of superbolt-class detections by the photodiode detector (PDD:

168   Kirkland et al., 2001) on the Fast On-Orbit Detection of Transient Events (FORTE) satellite

169   added additional evidence that superbolt-class detections might not describe extraordinary

170   lightning. Lightning pulses are broadened temporally by scattering in the cloud, yet the widths of

171   Kirkland's superbolt pulses were considerably narrow compared to normal lightning. This

172   suggests that the emissions took a relatively clear path to the satellite. Coincident NLDN

173   measurements during FORTE PDD superbolts over the United States between April and

174   September 1998 further showed that these highly-energetic optical pulses were generated by both

175   positive- and negative-polarity CGs whose peak currents were as low as 10 kA. Superbolt cases

176   were ubiquitous across the lightning-producing regions of the world (i.e., not concentrated in an

177   anomalous region or season) including the tropical lightning hotspots (Albrecht et al., 2016).

178   Finally, the FORTE very high frequency (VHF) waveforms that accompanied the optical

179   superbolt detections had signatures of multiple types of CG and IC processes (Light et al.,

180   2001b).

181   1.3 Anvil and stratiform superbolts

182   Kirkland's (1999) results do not eliminate the possibility that superbolts originate from a

183   unique type of lightning, but they show that unique flashes and thunderstorms do not hold a

184   monopoly on extremely bright optical pulses. Peterson et al. (2020b) also demonstrated this by

185   quantifying superbolt frequency in LIS measurements from the Tropical Rainfall Measuring

186   Mission (TRMM: Kummerow et al., 1998) satellite according to the Precipitation Radar (PR)

187   reported cloud type in the region illuminated by the flash. The most energetic optical pulses

188   recorded by LIS typically occurred in one of two scenarios: "anvil superbolts" where most of the

189   illuminated pixels were located near cloud boundaries outside of the raining area of the storm,

190   and "stratiform superbolts" that almost exclusively illuminated raining stratiform clouds.

191   Peterson et al. (2020b) also used continuous Geostationary Lightning Mapper (GLM:

192   Goodman et al., 2013; Rudlosky et al., 2019) observations to examine how lightning

193   characteristics changed over time within a single storm system. These analyses showed that early

194   convection was favorable for large flashes that lacked apparent lateral motion. Such flashes

195   could illuminate large portions of the convective anvil as well as neighboring clouds due to their

196   brightness combined with proximity to the storm edge – occasionally leading to anvil superbolts.

197   Upscale growth and organization into an MCS eroded this proximity to the storm edge, causing

198   large-stationary flashes to become overshadowed by the horizontally-propagating stratiform

199   lightning flashes that are associated with stratiform superbolts.

200   The TRMM and GLM data in Peterson et al. (2020b) supported both interpretations of

201   superbolt origins. There exists a class of superbolts where favorable viewing conditions allow

202   normal lightning to be particularly radiant. However, there is also a class of superbolts associated

203   with a particular type of lightning (strong peak current +CGs) that results from a unique set of

204   physics. Unfortunately, LIS is an integrating instrument that lacks the necessary time resolution

205   to resolve superbolts based on peak optical power, and this made drawing parallels with

206   Turman's (1977) sample of superbolts difficult.

207   The present study uses high-speed PDD detections over the complete FORTE dataset

208   (1997-2010) to identify superbolt-class optical lightning events around the world, and coincident

209   RF data to investigate their origins. We hypothesize that the brightest optical emissions from

210   lightning (> 350 GW at the source) come from +CGs, while weaker superbolts (100 GW – 350

211   GW) result from both normal lightning with favorable viewing conditions and +CGs. While

212   there is certainly a subset of superbolt-class detections that does not warrant distinction due to

213   their dependence on how the signals are measured, we propose that the term is justified for the

214   +CG cases.

215   **2 Data and Methodology**

216   A combination of optical and RF measurements is used to examine optical lightning

217   superbolts. These measurements were provided primarily by the FORTE satellite (Light et al.,

218   2001b; Kirkland et al., 2001). NLDN measurements from across North America during the

219   FORTE mission are also leveraged to add peak current and polarity information to the optical

220   events recorded by FORTE. We do not show waveforms from FORTE's RF payload because the

221   superbolts at the 10^{12} W peak optical power level either had NLDN coincidence or occurred

222   when the RF payload was inoperable (starting in 2003). Section 2.1 describes the FORTE optical

223   sensor package while Section 2.2 outlines our methodology for distinguishing lightning

224   superbolts in the space-based optical measurements.

225   *2.1 The FORTE Sensor Package*

226   The FORTE satellite carried multiple detectors that provided a wealth of information

227   about its recorded lightning events. FORTE's Optical Lightning System (OLS) consisted of two

228   instruments: the Lightning Locating System (LLS), and the Photodiode Detector (PDD). These

229   instruments recorded the steady-state background radiance of the cloud scene and then triggered

230   on transient optical pulses caused by lightning illuminating the clouds or other phenomena that

231   resemble lightning.

232   The LLS was based on the LIS design with hardware provided by NASA Marshall Space

233   Flight Center. It had a lower frame rate than LIS (a nominal 405 FPS compared to 500 FPS), and

234   the relatively high 800-km orbit of FORTE resulted in a pixel size of 10 km projected to ground.

235   The key difference between LLS and LIS lies in how the stream of event detections was

236   processed. The LLS did not use LIS signal processing techniques, but instead employed a

237   module designed by Sandia National Laboratories. Single-pixel, single integration-frame triggers

238   known as "events" in the LIS community were not clustered into more complex lightning

239   features representing lightning flashes during the FORTE mission.

240   The second instrument in FORTE's optical payload was the PDD. The PDD was a high-

241   speed (66,667 FPS) broadband (0.4–1.1 μm) photodiode detector that recorded 2–6 ms records

242   that integrate all lightning activity across its 80° FOV. FORTE's PDD may be the closest analog

243   to the original Vela instrumentation that reported the first superbolts. However, the FORTE PDD

244   had two key limitations that could prevent detection in certain scenarios: (1) there was a dead

245   time after each trigger that was approximately equal to the record length, and (2) only a specific

246   number of successive triggers could be recorded over a short time. The exact number depends on

247   the instrument configuration, but limits of 10 or 20 are common. This record limit is the more

248   restrictive caveat of the two because +CGs are often preceded by extensive cloud activity that

249   can trigger the PDD. In these cases, the PDD might exhaust its record limit before the return

250   stroke that would produce the superbolt.

251   In addition to recording lightning, the PDD was also known to trigger on energetic

252   particle impacts and other non-lightning events that produced waveforms that are inconsistent

253   with lightning behavior. Kirkland et al. (2001) documented a collection of filters that remove

254   non-lightning triggers from the PDD dataset. We apply these methods to the full PDD data

255   record used in this study to screen for artifacts.

256

257   *2.2 Identifying Optical Superbolts*

258   Superbolts have generally been identified by choosing a somewhat arbitrary energy

259   threshold in the top 1% of lightning emissions, and then classifying anything above that

260   threshold as a superbolt. For the FORTE PDD, we leverage the methodology used by Turman

261   (1977) and Kirkland (1999) to identify superbolts. The optical waveforms recorded at the

262   satellite are used to compute peak optical powers and total radiated energies at a source that is

263   assumed to be directly below the satellite. PDD events with peak optical powers at the source

264   that exceed 10^{11} W are classified as superbolts.

265   Lightning imagers (LIS, LLS) lack the high frame rates required to measure the peak

266   optical power of the lightning pulse. Entire waveforms recorded by the PDD are captured in a

267   single LLS frame. LIS / LLS capture photons throughout the frame duration and then report the

268   total received radiance over this time at readout. "Superbolts" that are identified based on pulse

269   total energy measurements (Peterson et al., 2017c, Holzworth et al., 2019) may not be the same

270   as Turman's (1977) superbolts identified based on peak optical power.

271   Fortunately, the FORTE PDD waveforms allow us to test whether superbolt thresholds

272   based on energy and power describe the same flashes. Figure 1 shows two-dimensional

273   distributions of PDD peak power against total integrated energy for the most radiant PDD events.

274   Both parameters are normalized to estimate the emission at the source rather than the radiance

275   received at the satellite. The thatched regions in the plot signify superbolts determined by peak

276   optical power (>100 GW) or total integrated energy (10^8 J). Events in the double-thatched region

277   to the top right of the plot meet both criteria.

278   There were 20,283 PDD superbolt-class events across the globe based on peak optical

279   power (>100 GW) of acceptable quality, representing the top 0.21% of the 9.3 million PDD

280   lightning detections. This fraction matches Turman's (1977) proportion of superbolts at the 100

281   GW level. Increasing the threshold drastically reduces the sample size. By 350 GW, only 1086

282   PDD events remain comprising 0.011% of all lighting. The proportion of 3-TW events in the

283   Vela data documented by Turman (1977) suggests that the FORTE PDD should have detected ~4

284   of these events over its mission. The PDD actually detected two such events, but waveform

285   analyses suggest that one of them is a Hyper-velocity Microgram Particle Impact (HMPI) at the

286   satellite rather than a terrestrial lightning source.

287   Figure 1 shows how the superbolts identified based on total optical energy differ from

288   those identified by peak optical power. For each peak optical power level (for example, 10^{10} W),

289   there is a range of approximately 1-2 orders of magnitude in the associated total optical energy

290   due to varying pulse widths and the limited millisecond-scale record lengths. Defining an energy

291   threshold (say, 10^8 J) will still capture the 100-GW peak power superbolts with the broadest

292   peaks, but the majority of the peak-power superbolts will be missed.

293   The brightest events in terms of total optical energy are still superbolts, but they do not

294   represent *all* of the superbolts. Particularly quick events, -CGs for example, will be missed

295   because they do not radiate for a long enough period to reach this total energy threshold. Thus,

296   instruments like LIS (Peterson et al., 2017c) and GLM (Peterson, 2019a) will excel at finding

297   +CG superbolts with their broader pulses, but may have difficulty identifying other types.

298   **3 Results**

299   The FORTE PDD provides similar representations of optical lightning pulses to the Vela

300   optical system. For this reason, the high-energy events reported by FORTE will be a more

301   appropriate analog to Turman's (1977) superbolt observations compared to superbolts identified

302   by other types of measurement types. In the following sections, we document where and when

303   these energetic optical pulses occur, and what types of lightning produce them.

304   *3.1 NLDN measurements of superbolt flashes*

305   We first examine the polarities and peak currents of the NLDN strokes that accompany

306   superbolt-class PDD events. Kirkland's (1999) NLDN analysis of PDD events over North

307   America between April and September 1998 showed that both +CGs and -CGs could generate

308   >100 GW events. The NLDN data suggested that even relatively weak strokes with peak currents

309   < 20 kA could produce superbolts. This view is not supported by Holzworth et al. (2019) whose

310   Earth Networks Global Lightning Network (ENGLN) peak current distribution lacks superbolt

311   cases below 100 kA.

312   The most likely reason for this discrepancy is because the WWLLN superbolts identified

313   by Holzworth et al. (2019) are measured by RF instruments rather than optically. It is thus not

314   guaranteed (and probably unlikely) that they capture the same sample of lightning events as

315   Turman (1977). Kirkland's PDD (1999) analysis supports the idea that particularly favorable

316   sight lines can cause many types of lightning to produce superbolts, but RF measurements such

317   as those provided by WWLLN and ENGLN are not modified by the clouds in this way. For

318   WWLLN to record a high-energy stroke, it must be a strong CG. Since the ENGLN peak current

319   threshold for matched WWLLN superbolts is identical for +CGs and -CGs, both parameters

320   (ENGLN peak current and WWLLN energy) should be highly correlated. Peak current is

321   calculated from the Range-Normalized Signal Strength (RNSS) of a geolocated source, and is a

322   measure of the peak E-field in the RF waveform. In this way, it is similar to the PDD peak

323   optical power of the source calculated from the maximum in the PDD waveform. WWLLN

324   energies, meanwhile, are calculated by integrating the E-field through the sferic, and are thus

325   similar to the PDD total optical energy. Holzworth's (2019) comparisons between peak current

326   and WWLLN energy are then, essentially, an RF analog to our Figure 1 for the FORTE PDD,

327   and it is not surprising to see that RF-detected superbolts generate powerful emissions recorded

328   by both RF networks.

329   However, the other issue that both studies share is their limited sample size of superbolt-

330   class event coincidence with the ground networks that report peak current. Kirkland (1999)

331   identified just 130 superbolt cases coincident with NLDN, while Holzworth et al. (2019) found

332   just 18 matches with ENGLN. It is unclear whether either analysis is truly representative.

333   To generate more robust statistics, we repeat Kirkland's (1999) approach for identifying NLDN

334   matches to PDD events and extend it to the whole FORTE record (1997 – 2010). NLDN

335   observations are limited to a domain surrounding the United States. These matches are only

336   representative of the global PDD dataset under the assumption of identical physics across all

337   terrestrial strokes. Figure 2a shows the population density of all of our 3.1×10^4 NLDN-matched

338   PDD events. Figure 2b shows the average peak current for the PDD / NLDN matches. PDD peak

339   optical power generally correlates with NLDN peak current, and the strokes associated with

340   superbolts exceed 80 kA, on average. For a given peak optical power, however, the NLDN peak

341   current tends to decrease as the total energy increases. In other words, lower peak currents are

342   required to generate bright optical pulses (in terms of peak optical power) that have longer-

343   duration pulses and higher total energies than quicker events. Finally, we compute the fraction of

344   all NLDN matches that are +CGs in Figure 2c. For non-superbolt cases, the +CG fractions at a

345   given peak-power increase from < 10% of all lightning in the lowest-energy (quickest) events to

346   50-100% of all lightning in the highest energy (longest-lasting) events. This supports the idea

347   that LIS / GLM superbolts identified based on total optical energy are more likely to be +CGs

348   than those identified by peak optical power.

349   Since the low sample sizes at each gridpoint in the superbolt domain of Figure 2 obscure

350   the peak current and polarity trends, Figure 3 accumulates all PDD / NLDN matched events

351   above certain PDD optical power levels and constructs histograms (bar plots) and Cumulative

352   Density Functions (lines) for each level. The histograms are normalized according to the total

353   number of PDD / NLDN matches: positive-polarity (yellow) plus negative-polarity (blue). Figure

354   3a shows the distributions for all PDD matches from Figure 2. These matches are most

355   frequently 10 - 30 kA NLDN strokes (median: -21 kA, +14 kA), primarily -CGs. Figure 3b

356   subsets the sample to only include PDD / NLDN matches where the peak optical power at the

357   source exceeds 100 GW. The inclusion of both positive and negative strokes as well as the

358   overall -CG dominance agrees with Kirkland's (1999) and Holzworth's (2019) findings.

359   However, the peak currents for these 100 GW optical superbolts are notably higher than

360   Kirkland's (1999) assessment with mean values of -73 kA and +103 kA, though still weaker than

361   the superbolt peak current range in Holzworth et al. (2019).

362   If we continue increasing the PDD peak power threshold to only capture stronger events,

363   we start to see the -CG peak erode until it is overtaken by the +CG peak. By 350 GW (Figure

364   3c), the histogram is dominated by +CGs that exceed 100 kA (mean: +133 kA). This change

365   shows that the superbolts at 100 GW are generated by a different set of lightning processes than

366   those at higher peak powers. It is thus possible that Kirkland's (1999) assessment from NLDN

367   events and FORTE VHF waveforms that positive and negative CG and IC pulses may generate

368   superbolts is correct at the 100 GW level, while terawatt-scale superbolts only occur in certain

369   circumstances enabled by the dynamics and charge structure of the parent thunderstorm.

370

371   *3.2 Global and seasonal distributions of FORTE PDD superbolts*

372   To gauge where superbolts at different source peak power levels come from, we construct

373   global distributions for the FORTE satellite subpoint locations during these radiant PDD events.

374   These maps do not capture accurate source locations because the emitter could be located

375   anywhere across PDD's FOV that is ~1200 km across. In cases where we have LLS coincidence

376   with the PDD, we can geolocate the source to within 10 km, but many of our superbolt cases

377   occurred while the LLS was not reporting. Thus, only 9.3% of the 100 GW superbolts occur

378   alongside an LLS event.

379   Figure 4 shows the distribution of FORTE positions during PDD superbolts whose peak

380   optical powers exceeded 100 GW at the source. As in Kirkland's (1999) analysis, these sources

381   are distributed broadly across the globe with high concentrations of events near the tropical

382   chimney regions in South America, central Africa, and the Maritime Continent in Asia. Weaker

383   local maxima can also be noted leeward of the major continents, and in the Mediterranean Sea.

384   Many of these regions were identified by Holzworth et al. (2019) as hotspots for WWLLN

385   superbolt activity, though clear maxima over the Andes and in the North Sea are not evident in

386   the optical PDD data.

387   As with the NLDN peak current histograms in Figure 3, increasing the peak power

388   threshold changes the global distribution of superbolt cases. Figure 5 maps the global distribution

389   of all cases whose peak powers at the source exceeds 350 GW (as in Figure 3c). The maxima

390   near the tropical chimneys disappear entirely, leaving a few scattered (primarily oceanic) cases

391   across the tropics. The previously-secondary peaks along the Gulf Stream, in the Mediterranean,

392   and surrounding Japan become the most prominent features in the distribution – with the Sea of

393   Japan / North Pacific Ocean further east producing more superbolts than any other region across

394   the globe.

395   The seasonal cycles for these superbolt flashes also change based on the peak optical

396   power threshold. Figure 6 plots the frequency of superbolts ranging from 100 GW to 500 GW for

397   each month of the year in the northern mid-latitudes (Figure 6a), the tropics (Figure 6b) and the

398   southern mid-latitudes (Figure 6c). There are two distinct maxima in the seasonal cycle for 100

399   GW superbolts in the northern mid-latitudes (Figure 6a): one in July, and another in December.

400   The tropical curves (Figure 6b) are mostly flat over the year with three peaks at lower energies

401   (March, July, and October). The southern hemisphere curves (Figure 6c) all have a single

402   pronounced wintertime peak. The northern hemisphere summer peak declines as we move up in

403   power, however. It is no longer the annual maximum by 150 GW, and is indistinguishable in the

404   300 GW and 500 GW curves. At these higher peak optical powers, subtropical superbolts are

405   dominated by winter lightning in both hemispheres, in agreement with the WWLLN statistics

406   shown in Holzworth et al., (2019).

407   The fact that maxima in the lightning distributions flip from the tropics to the subtropics

408   and from summer to winter between 100 GW and 350 GW provides further support that the

409   composition of the lightning sample is highly sensitive to the selected peak optical power

410   threshold. The relatively weak cases at 100 GW appear to comprise a diverse sample of "normal"

411   lightning, but the 350+ GW superbolts predominantly occur in wintertime oceanic storms that

412   are known for strong +CGs.

413   *3.3 The most radiant superbolts observed by the FORTE PDD*

414   Our previous analyses have stopped at 350 GW due to the limited number of cases above

415   this peak power level. The FORTE PDD did measure superbolts that were more radiant,

416   however. There were a total of 38 PDD events that reached the terawatt scale, and these are

417   listed in Table 1. Because peak optical power and total integrated optical energy are correlated

418   (i.e., Figure 1), all of these cases generated at least 10^8 J of energy with effective pulse widths

419   ranging from 155 µs to 542 µs. Nine of the 38 events were detected exclusively by the PDD with

420   no other FORTE sensor reporting. This was particularly commonplace after the RF payload

421   became inoperable in 2003. There were 4 events that occurred over North America and all four

422   had NLDN coincidence. NLDN reported peak currents ranged from 94 kA to 167 kA and were

423   all cases of positive-polarity return strokes.

424   The overall brightest superbolt recorded by the PDD had a peak optical power at the

425   source of 3.14×10^{12} W, a total integrated source energy of 7.99×10^8 J, and an effective pulse

426   width of 255 µs. The PDD waveform for this event is shown in Figure 7. The light curve builds

427   quickly to its initial peak, and then optical emission persists for at least 1.3 ms afterwards. The

428   PDD record ends before the radiance reached the background value. The slowly-varying weak

429   emissions appear to be continuing current from the CG.

430

431   **4 Summary**

432   We use the full FORTE PDD record (1997-2010) to identify optical superbolts and

433   examine the types of lightning that produce them. We find that the weaker superbolts (10^{11} W)

434   analyzed by Turman (1977) in the Vela data and Kirkland (1999) in the FORTE PDD data result

435   from a variety of lightning types. Many of these are not exceptional cases of lightning, but

436   instead normal lightning that happens to have a clear sight line to the sensor. However, the

437   brighter events that have coincidence with ground-based measurements - including some

438   terawatt-scale detections – are predominantly intense +CG strokes. These brightest events result

439   from unique thunderstorm dynamics that are often found in oceanic storms, particularly during

440   the winter, and especially surrounding the Japanese archipelago and Mediterranean Sea.

441   The frequency and intensity of FORTE PDD superbolts is found to be consistent with

442   Turman's (1977) results from the Vela constellation, though our results are limited by the fact

443   that FORTE was a single satellite in low Earth orbit. Terawatt-class superbolts are exceptionally

444   rare phenomena. In 12 years of on-orbit operations, the FORTE PDD only detected one valid

445   lightning case that exceeded Turman's (1977) 3-TW threshold. Staring coverage from a high-

446   speed optical instrument in a geosynchronous orbit would allow these events to be readily

447   detected. The upcoming LANL/SNL/NNSA SENSER payload will feature instrumentation

448   similar to the FORTE sensor package in a western hemisphere geosynchronous orbital slot that

449   should allow these exceptionally-bright cases to be detected and compared with space-based

450   lightning imagers (GLM, LIS), long-range ground-based networks (NLDN, WWLLN, ENTLN),

451   and regional Lightning Mapping Arrays (LMAs) across the Americas. While only some of the

452   Earth's superbolt hotspots will be observed by all of these instruments, this wealth of data will

453   enable unprecedented examinations of the physics behind these interesting lightning events – and

454   perhaps finally settle the debate as to whether certain flashes merit the distinction of

455   "superbolts."

456

Acknowledgments

462

463 **References**

464   Albrecht, R. I., Goodman, S. J., Buechler, D. E., Blakeslee, R. J., & Christian, H. J. (2016).

465   Where are the lightning hotspots on Earth?. *Bulletin of the American Meteorological*

466   *Society*, *97*(11), 2051-2068.

467   Berger, K., & Vogelsanger, E. (1969). New results of lightning observations. *Planetary*

468   *Electrodynamics*, *1*(S 489).

469   Blanc, E., Farges, T., Brebion, D., Belyaev, A. N., Alpatov, V. V., Labarthe, A., & Melnikov, V.

470   (2007). Main results of LSO (Lightning and Sprite Observations) on board of the

471   International Space Station. *Microgravity Science and Technology*, *19*(5-6), 80-84.

472   Cecil, D. J., Buechler, D. E., & Blakeslee, R. J. (2014). Gridded lightning climatology from

473   TRMM-LIS and OTD: Dataset description. *Atmospheric Research*, *135*, 404-414.

474   Christian, H. J., R. J. Blakeslee, S. J. Goodman, and D. M. Mach (Eds.), (2000). Algorithm

475   Theoretical Basis Document (ATBD) for the Lightning Imaging Sensor (LIS),

476   NASA/Marshall Space Flight Center, Alabama. (Available as

477   http://eospso.gsfc.nasa.gov/atbd/listables.html, posted 1 Feb. 2000)

478   Cummins, K. L., Murphy, M. J., Bardo, E. A., Hiscox, W. L., Pyle, R. B., & Pifer, A. E. (1998).

479   A combined TOA/MDF technology upgrade of the US National Lightning Detection

480   Network. *Journal of Geophysical Research: Atmospheres*, *103*(D8), 9035-9044.

481   Goodman, S. J., Blakeslee, R. J., Koshak, W. J., Mach, D., Bailey, J., Buechler, D., ... & Stano,

482   G. (2013). The GOES-R geostationary lightning mapper (GLM). *Atmospheric research*,

483   *125*, 34-49.

484   Hayakawa, M., Nakamura, T., Hobara, Y., & Williams, E. (2004). Observation of sprites over

485   the Sea of Japan and conditions for lightning-induced sprites in winter. *Journal of*

486   *Geophysical Research: Space Physics*, *109*(A1).

487   Holzworth, R. H., McCarthy, M. P., Brundell, J. B., Jacobson, A. R., & Rodger, C. J. (2019).

488   Global distribution of superbolts. *Journal of Geophysical Research: Atmospheres*,

489   *124*(17-18), 9996-10005.

490   Kirkland, M. W. (1999). An examination of superbolt-class lightning events observed by the

491   FORTE satellite. *Los Alamos National Laboratory, Atmospheric Sciences Group, New*

492   *Mexico*.

493   Kirkland, M. W., Suszcynsky, D. M., Guillen, J. L. L., & Green, J. L. (2001). Optical

494   observations of terrestrial lightning by the FORTE satellite photodiode detector. *Journal*

495   *of Geophysical Research: Atmospheres*, *106*(D24), 33499-33509.

496   Kummerow, C., Barnes, W., Kozu, T., Shiue, J., & Simpson, J. (1998). The tropical rainfall

497   measuring mission (TRMM) sensor package. *Journal of atmospheric and oceanic*

498   *technology*, *15*(3), 809-817.

499   Lang, T. J., Rutledge, S. A., & Wiens, K. C. (2004). Origins of positive cloud-to-ground

500   lightning flashes in the stratiform region of a mesoscale convective system. *Geophysical*

501   *research letters*, *31*(10).

502   Lang, T. J., Pédeboy, S., Rison, W., Cerveny, R. S., Montanyà, J., Chauzy, S., ... & Carbin, G.

503   (2017). WMO world record lightning extremes: Longest reported flash distance and

504   longest reported flash duration. *Bulletin of the American Meteorological Society*, *98*(6),

505   1153-1168.

506   Light, T. E., Suszcynsky, D. M., Kirkland, M. W., & Jacobson, A. R. (2001). Simulations of

507   lightning optical waveforms as seen through clouds by satellites. *Journal of Geophysical*

508   *Research: Atmospheres*, *106*(D15), 17103-17114.

509   Lund, I. A. (1973). *Joint Probabilities of Cloud-Free Lines-of-Sight through the Atmosphere at*

510   *Grand Forks, Fargo, and Minot, North Dakota* (No. AFCRL-TR-73-0178). AIR FORCE

511   CAMBRIDGE RESEARCH LABS LG HANSCOM FIELD MASS.

512   Mach, D. M., Blakeslee, R. J., Bateman, M. G., & Bailey, J. C. (2010). Comparisons of total

513   currents based on storm location, polarity, and flash rates derived from high-altitude

514   aircraft overflights. *Journal of Geophysical Research: Atmospheres*, *115*(D3).

515   Mach, D. M., Blakeslee, R. J., & Bateman, M. G. (2011). Global electric circuit implications of

516   combined aircraft storm electric current measurements and satellite-based diurnal

517   lightning statistics. *Journal of Geophysical Research: Atmospheres*, *116*(D5).

518   Mazur, V., Shao, X. M., & Krehbiel, P. R. (1998). "Spider" lightning in intracloud and positive

519   cloud-to-ground flashes. *Journal of Geophysical Research: Atmospheres*, *103*(D16),

520   19811-19822.

521   Miyake, K., Suzuki, T., & Shinjou, K. (1992). Characteristics of winter lightning current on

522   Japan Sea coast. *IEEE Transactions on power Delivery*, *7*(3), 1450-1457.

523   Pasko, V. P., Inan, U. S., Taranenko, Y. N., & Bell, T. F. (1995). Heating, ionization and upward

524   discharges in the mesosphere, due to intense quasi-electrostatic thundercloud fields.

525   *Geophysical Research Letters*, *22*(4), 365-368.

526   Pasko, V. P., Inan, U. S., Bell, T. F., & Taranenko, Y. N. (1997). Sprites produced by quasi-

527   electrostatic heating and ionization in the lower ionosphere. *Journal of Geophysical*

528   *Research: Space Physics*, *102*(A3), 4529-4561.

529   Peterson, M., & Liu, C. (2013). Characteristics of lightning flashes with exceptional illuminated

530   areas, durations, and optical powers and surrounding storm properties in the tropics and

531   inner subtropics. *Journal of Geophysical Research: Atmospheres*, *118*(20), 11-727.

532   Peterson, M., Deierling, W., Liu, C., Mach, D., & Kalb, C. (2017a). A TRMM/GPM retrieval of

533   the total mean generator current for the global electric circuit. *Journal of Geophysical

534   Research: Atmospheres*, *122*(18), 10-025.

535   Peterson, M., Deierling, W., Liu, C., Mach, D., & Kalb, C. (2017b). The properties of optical

536   lightning flashes and the clouds they illuminate. *Journal of Geophysical Research:

537   Atmospheres*, *122*(1), 423-442.

538   Peterson, M., Deierling, W., Liu, C., Mach, D., & Kalb, C. (2018). A TRMM assessment of the

539   composition of the generator current that supplies the Global Electric Circuit. *Journal of

540   Geophysical Research: Atmospheres*, *123*(15), 8208-8220.

541   Peterson, M. (2019a). Research applications for the Geostationary Lightning Mapper operational

542   lightning flash data product. *Journal of Geophysical Research: Atmospheres*, *124*(17-18),

543   10205-10231.

544   Peterson, M. (2019b). Using lightning flashes to image thunderclouds. *Journal of Geophysical

545   Research: Atmospheres*, *124*(17-18), 10175-10185.

546   Peterson, M. J., Lang, T. J., Bruning, E. C., Albrecht, R., Blakeslee, R. J., Lyons, W. A., ... &

547   Cerveny, R. S. (2020a). New WMO Certified Megaflash Lightning Extremes for Flash

548   Distance (709 km) and Duration (16.73 seconds) recorded from Space. *Geophysical

549   Research Letters*, e2020GL088888.

550   Peterson, M., Rudlosky, S., & Zhang, D. (2020b). Changes to the appearance of optical lightning

551   flashes observed from space according to thunderstorm organization and structure.

552   *Journal of Geophysical Research: Atmospheres*, *125*(4), e2019JD031087.

553   Peterson, Michael, 2020, "Lightning Superbolt Data", https://doi.org/10.7910/DVN/RV39JT,

554   Harvard Dataverse, V1, UNF:6:EfCsUFiynHfRVOcQbMEWgA== [fileUNF]

555   Rakov, V. A. (2003). A review of positive and bipolar lightning discharges. *Bulletin of the*

556   *American Meteorological Society*, *84*(6), 767-776.

557   Rudlosky, S. D., Goodman, S. J., Virts, K. S., & Bruning, E. C. (2019). Initial geostationary

558   lightning mapper observations. *Geophysical Research Letters*, *46*(2), 1097-1104.

559   Rust, W. D., MacGorman, D. R., & Arnold, R. T. (1981). Positive cloud-to-ground lightning

560   flashes in severe storms. *Geophysical Research Letters*, *8*(7), 791-794.

561   Thomas, R. J., Krehbiel, P. R., Rison, W., Hamlin, T., Boccippio, D. J., Goodman, S. J., &

562   Christian, H. J. (2000). Comparison of ground-based 3-dimensional lightning mapping

563   observations with satellite-based LIS observations in Oklahoma. *Geophysical research*

564   *letters*, *27*(12), 1703-1706.

565   Turman, B. N. (1977). Detection of lightning superbolts. *Journal of Geophysical Research*,

566   *82*(18), 2566-2568.

567   Yamamoto, M. K., Higuchi, A., & Nakamura, K. (2006). Vertical and horizontal structure of

568   winter precipitation systems over the western Pacific around Japan using TRMM data.

569   *Journal of Geophysical Research: Atmospheres*, *111*(D13).

570

571
572
573
574

575
576

577 **Table 1.** Terawatt-class lightning superbolt cases detected by the FORTE PDD between 1997
578 and 2010. Only one case reached the 3-TW level, like the cases listed by Turman [1977]. All
579 four cases around CONUS (shaded yellow) had NLDN coincidence and resulted from +CG
580 return strokes. Reported peak currents (from top-down) were +168 kA, +95 kA, +175 kA, and
581 +161 kA, respectively.
582

DATE	UTC TIME	PDD LON	PDD LAT	PEAK POWER [W]	TOTAL ENERGY [J]	PULSE WIDTH [µs]	LLS OR RF MATCH?	NLDN MATCH?
07/31/99	10:10:38.73	30.5	-33.1	1.03E+12	4.71E+08	458	YES	N/A
02/05/00	18:14:16.43	-170.0	45.6	1.03E+12	3.51E+08	341	NO	N/A
01/28/03	10:07:10.34	49.4	29.6	1.03E+12	3.69E+08	359	YES	N/A
05/23/03	22:43:53.52	27.8	-28.9	1.03E+12	3.98E+08	387	NO	N/A
12/23/05	00:49:36.80	-150.3	33.7	1.03E+12	3.40E+08	331	YES	N/A
12/30/97	09:32:19.48	-74.7	29.6	1.08E+12	3.62E+08	336	YES	YES
08/14/04	06:10:02.81	-73.3	21.4	1.08E+12	2.73E+08	253	YES	N/A
07/26/07	05:05:37.88	74.0	41.1	1.08E+12	3.15E+08	292	YES	N/A
06/13/99	21:10:16.49	-128.9	-42.1	1.13E+12	2.39E+08	212	NO	N/A
10/21/07	14:13:54.31	11.8	37.1	1.13E+12	5.77E+08	512	YES	N/A
12/18/98	12:13:01.42	-138.4	-47.5	1.18E+12	4.06E+08	346	YES	N/A
02/22/99	07:03:25.27	40.2	47.5	1.18E+12	3.87E+08	329	NO	N/A
03/25/01	09:02:37.16	-68.0	37.8	1.18E+12	5.56E+08	473	YES	YES
11/28/01	21:02:43.02	170.8	45.4	1.18E+12	2.99E+08	255	YES	N/A
01/31/03	12:11:48.02	1.2	41.8	1.18E+12	5.53E+08	470	YES	N/A
09/13/05	23:57:15.65	157.8	-34.4	1.18E+12	4.07E+08	346	YES	N/A
07/09/07	23:09:15.89	36.8	-43.9	1.18E+12	2.59E+08	220	NO	N/A
01/08/08	13:03:13.36	118.1	0.0	1.18E+12	3.06E+08	261	YES	N/A
07/05/07	15:07:10.85	-48.3	-43.4	1.23E+12	5.17E+08	422	NO	N/A
04/18/01	13:33:10.66	-68.0	39.2	1.27E+12	3.91E+08	307	YES	YES
12/13/04	00:31:46.46	148.2	10.5	1.27E+12	4.59E+08	361	YES	N/A
01/28/05	12:54:30.66	18.9	46.2	1.27E+12	5.26E+08	413	YES	N/A
01/18/09	04:14:01.16	131.0	36.2	1.27E+12	3.55E+08	278	YES	N/A
05/17/02	16:13:10.15	-87.8	35.8	1.32E+12	7.18E+08	542	YES	YES
06/12/99	09:14:11.62	3.2	55.9	1.42E+12	4.68E+08	329	NO	N/A
02/06/05	09:06:45.70	39.3	34.3	1.42E+12	4.59E+08	323	YES	N/A
04/03/05	14:30:30.49	136.1	33.5	1.42E+12	5.78E+08	407	YES	N/A
01/30/00	13:21:59.83	142.0	37.8	1.47E+12	4.00E+08	272	NO	N/A
11/24/05	06:38:18.99	5.1	36.6	1.47E+12	4.92E+08	335	NO	N/A
03/16/07	19:20:31.20	-111.1	-40.2	1.62E+12	4.01E+08	248	YES	N/A
05/07/02	19:02:58.14	48.0	40.1	1.86E+12	7.76E+08	417	YES	N/A
09/20/01	16:57:23.66	151.8	-57.6	1.91E+12	5.13E+08	268	YES	N/A
12/23/05	04:12:00.30	159.0	34.5	1.91E+12	4.68E+08	245	YES	N/A
05/15/02	16:13:17.67	101.9	-42.2	1.96E+12	3.07E+08	157	YES	N/A
12/07/05	02:52:24.32	14.6	44.8	2.01E+12	3.11E+08	155	YES	N/A
12/23/05	21:31:23.58	45.3	37.8	2.01E+12	4.89E+08	243	YES	N/A
06/10/01	14:26:40.10	75.5	64.2	2.16E+12	1.02E+09	475	YES	N/A
08/16/02	15:44:32.64	-111.5	-70.1	3.14E+12	7.99E+08	255	YES	N/A

583
584
585
586
587
588

589
590

Figure 1. Two-dimensional histogram of peak optical power (abscissa) and the total integrated energy at the source (ordinate) for the brightest PDD events. Superbolts defined by peak optical power (> 100 GW) and total energy (> 10^8 J) are thatched. Only events in the double-thatched top-right region are identified as superbolts by both power and energy criteria. Note that the steps in frequency at 20 GW and 300 GW are due to the piecewise linear dynamic range of the PDD discussed in Kirkland et al. (2001).

591
592
593
594
595
596
597
598
599
600
601
602
603
604
605
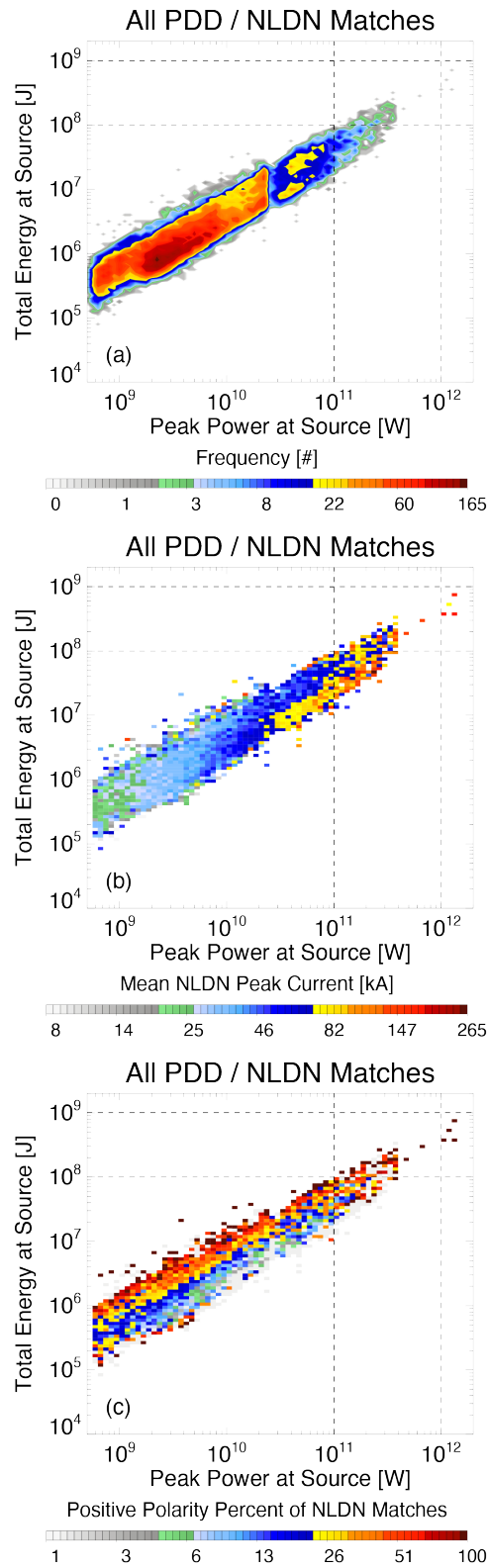
Figure 2. Two-dimensional histograms of peak optical power and the total integrated energy for PDD events with NLDN matches. Frequency (a), mean NLDN peak current (b), and the percent of NLDN matches that are positive-polarity (c) are shown.
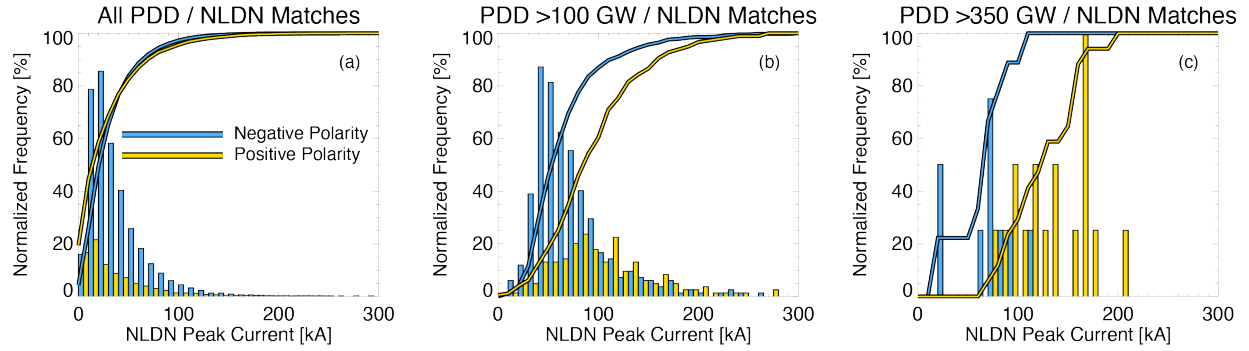
Figure 3. Histograms (bar graphs) and Cumulative Density Functions (lines) for the NLDN peak current associated with (a) all PDD / NLDN matches, (b) >100 GW PDD / NLDN matches, and (c) >350 GW PDD / NLDN matches. Most PDD matches occur with negative-polarity (blue) NLDN strokes, but high-energy superbolts (>350 GW) are disproportionately positive-polarity (yellow) NLDN strokes.
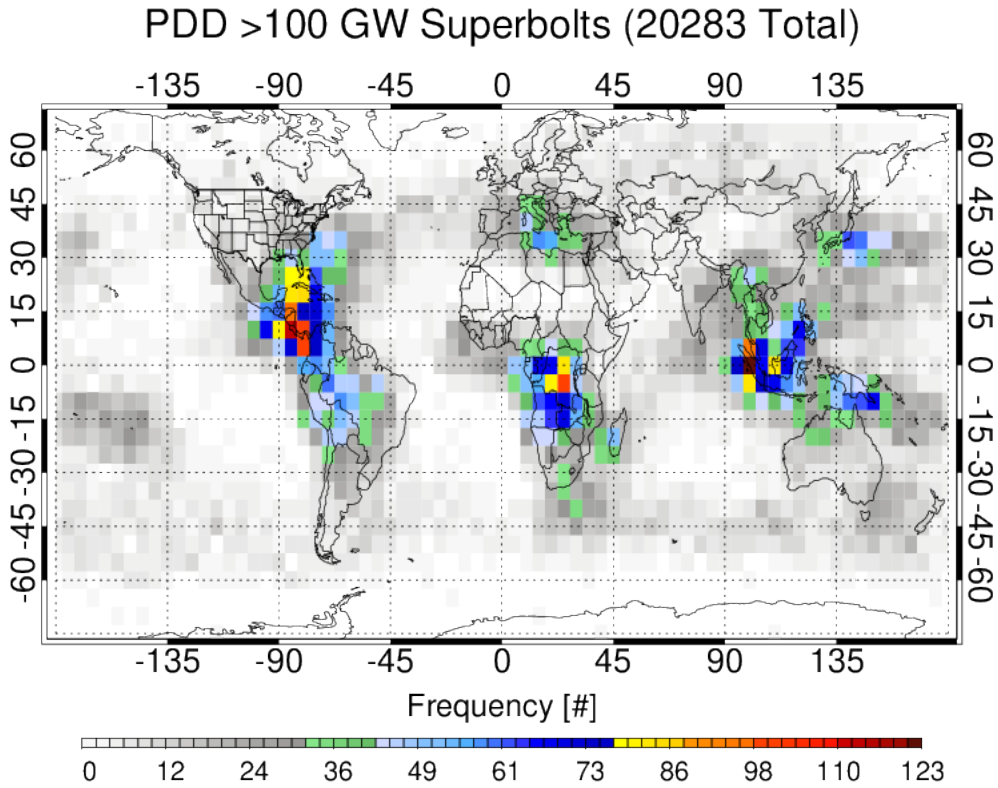
Figure 4. Global distribution of all PDD events whose peak powers at the source exceeds 100 GW. The highest concentration of superbolts are concentrated in the tropical chimney regions around Colombia / Venezuela in the Americas, the Congo Basin in Africa, and the Maritime Continent in Asia.
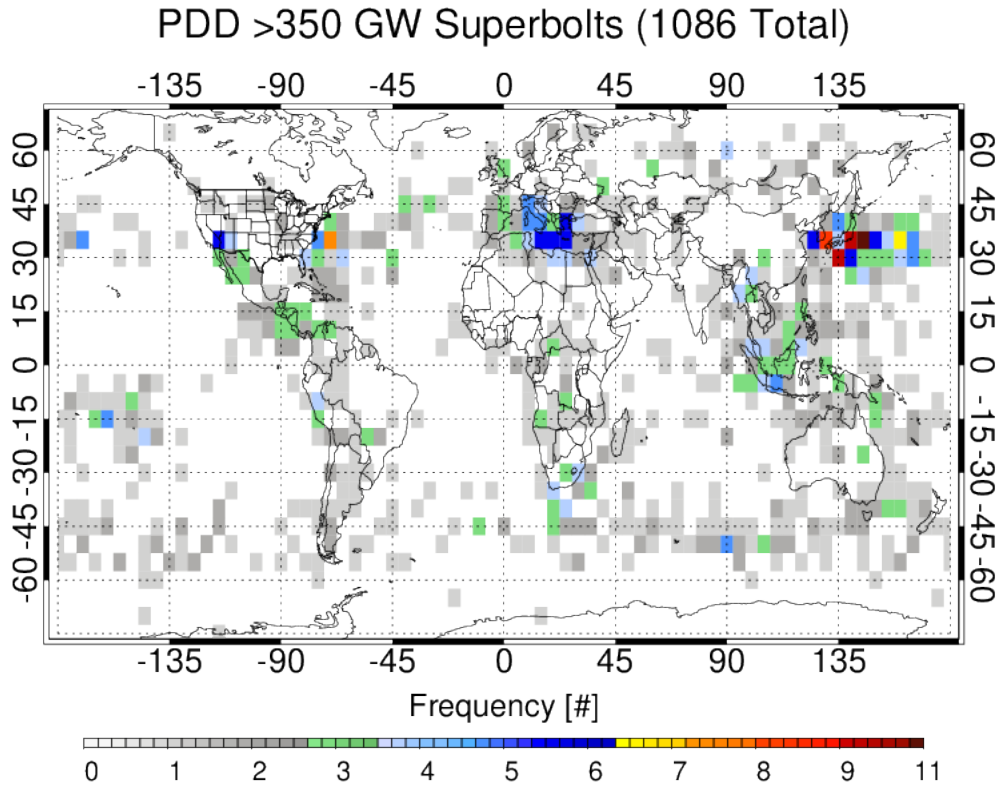
Figure 5. Global distribution of all PDD events whose peak powers at the source exceeds 350 GW. The highest concentrations of superbolt activity at this power level are found in the mid-latitudes, particularly in the Mediterranean Sea, the Sea of Japan, and the northern Pacific Ocean. Note that the contour levels are lower than in Figure 4 due to the decreased sample size.
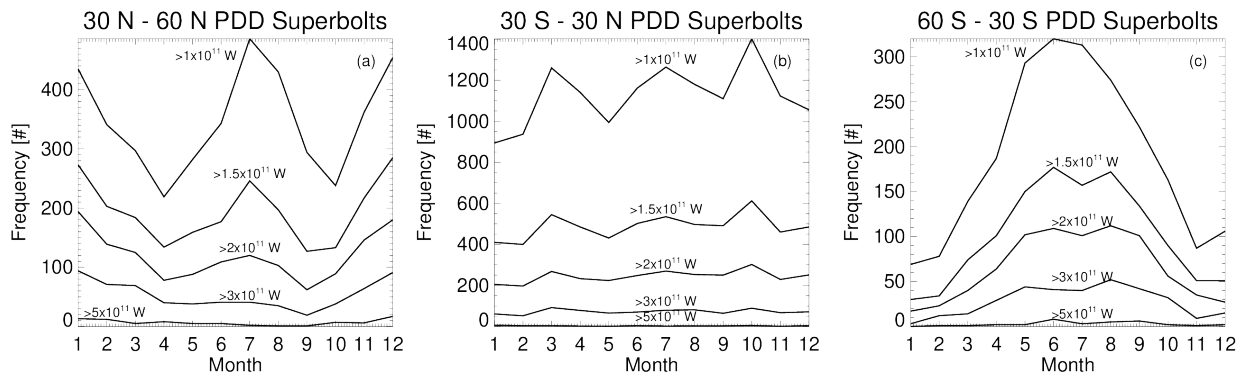
Figure 6. Annual cycles of superbolts activity over the (a) northern mid-latitudes, (b) the tropics, and (c) the southern mid-latitudes. Individual curves are drawn for various source peak power levels from 100 GW to 500 GW. Mid-latitude superbolt activity peaks in the winter months, but the northern hemisphere has a second summertime peak that erodes at higher power levels.
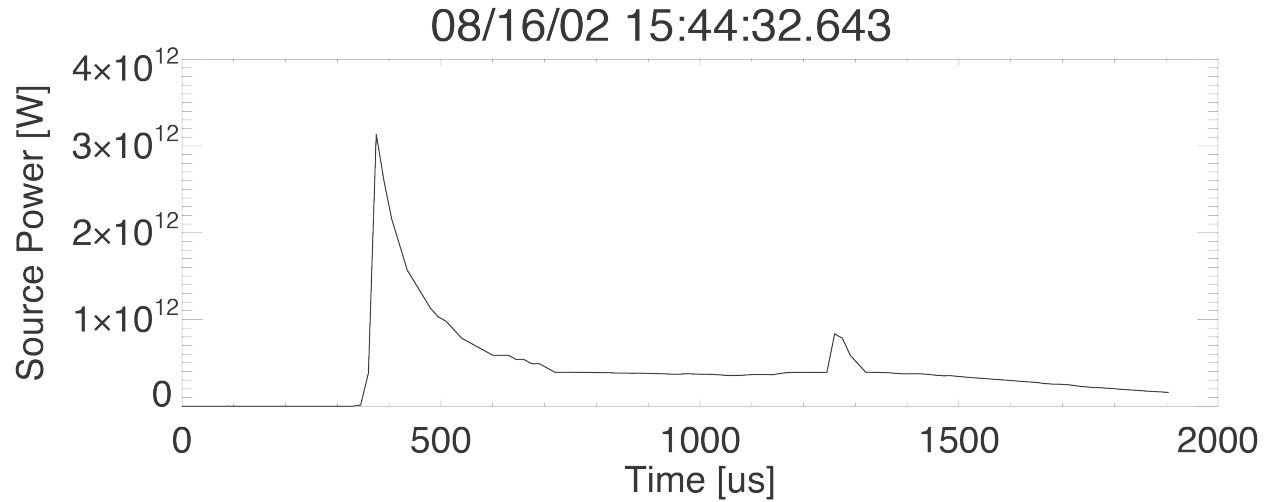
Figure 7. PDD optical waveforms from the most radiant superbolt case observed by FORTE. The intense peak was followed by 1.3 ms of continuous emission including a second weaker peak 1-ms after the first.